Süleyman Demirel Üniversitesi
Fen Bilimleri Enstitüsü Dergisi
Cilt 29, Sayı 2, 366-374, 2025

Süleyman Demirel University
Journal of Natural and Applied Sciences
Volume 29, Issue 2, 366-374, 2025

DOI: 10.19113/sdufenbed.1691010

Innovative Bioactive Zirconia Glass Ceramics: Combining Radiation Protection and Biocompatibility

Özge KILIÇOĞLU*[1]

[1]Marmara Üniversitesi, SHMYO, Tıbbi Görüntüleme Bölümü, 34865, İstanbul, Türkiye

(Alınış / Received: 03.05.2025, Kabul / Accepted: 27.06.2025, Online Yayınlanma / Published Online: 25.08.2025)

Keywords
Zirconia,
Glass Ceramics,
Radiation Shielding,
Mass attenuation coefficient,
Biocompatibility

Abstract: This study assesses the γ-ray shielding performance of zirconia-doped transparent glass-ceramics (TGCs) derived from the SiO_2–Na_2O–CaO–P_2O_5 system over 0.015–15 MeV. Four compositions (BG1–BG4, 0–6 mol % ZrO_2) were analysed using the Phy-X/PSD software and the PHITS-3.22 Monte Carlo code, which agreed closely; the largest deviation was 1.47 % for BG1 at 3 MeV while largest deviation is only 1.39 % for BG4 at 8 MeV. For BG4, the mass attenuation coefficient declined from 8.040 $cm^2 g^{-1}$ at 0.015 MeV to 0.022 $cm^2 g^{-1}$ at 15 MeV, while the half-value layer changed 0.0030–10.649 cm. BG4 also recorded the highest linear attenuation coefficient, 23.398 cm^{-1} at 0.015 MeV, and its HVL at 0.1 MeV was 16.7 % lower than BG1. Replacing CaO with 6 mol % ZrO_2 raised density from 2.535 to 2.910 g cm^{-3} (+14.8 %) and reduced molar volume, enhancing structural compactness and attenuation. Zirconia-rich TGCs—especially BG4—thus present environmentally benign, lead-free, and biocompatible options for radiation-shielded dental and orthopaedic implants.

Yenilikçi Biyoaktif Zirkonya Cam Seramikleri: Radyasyon Zırhlama ve Biyouyumluluğun Birleşimi

Anahtar Kelimeler
Zirkonya
Şeffaf cam seramik,
Radyasyon zırhlama,
Kütle zayıflatma katsayısı,
Biyouyumluluk

Öz: Bu çalışma, SiO_2–Na_2O–CaO–P_2O_5 sisteminden türetilen zirkonya katkılı şeffaf cam-seramiklerin (TGC) 0,015–15 MeV aralığındaki γ-ışını zırhlama performansını değerlendirmektedir. Dört bileşim (BG1–BG4, %0–6 mol ZrO_2) Phy-X/PSD yazılımı ve PHITS-3.22 Monte Carlo kodu kullanılarak analiz edilmiş olup sonuçlar büyük ölçüde uyumludur; en büyük sapma BG1 için 3 MeV'de %1,47 iken BG4 için 8 MeV'de yalnızca %1,39'dur. BG4 numunesinde kütle zayıflatma katsayısı 0,015 MeV'de 8,040 $cm^2 g^{-1}$'den 15 MeV'de 0,022 $cm^2 g^{-1}$'ye düşmüş, yarı değer kalınlığı 0,0030–10,649 cm aralığında değişmiştir. BG4 ayrıca 0,015 MeV'de 23,398 cm^{-1} ile en yüksek doğrusal zayıflatma katsayısını kaydetmiş ve 0,1 MeV'deki HVL değeri BG1'den %16,7 daha düşüktür. CaO'nun %6 mol ZrO_2 ile ikamesi yoğunluğu 2,535'ten 2,910 g cm^{-3}'e (+%14,8) yükseltmiş ve molar hacmi azaltarak yapısal sıkılığı ve zayıflatmayı artırmıştır. Zirkonya açısından zengin TGC'ler—özellikle BG4—bu nedenle radyasyon zırhlamalı diş ve ortopedik implantlar için çevre dostu, kurşunsuz ve biyouyumlu seçenekler sunmaktadır.

1. Introduction

Radiation shielding is essential in healthcare settings like radiology, dentistry, and oncology to safeguard patients and staff from harmful ionizing radiation. Lead has been the primary shielding material because of its high density and radiation attenuation capabilities. Nevertheless, its toxicity, environmental risks, and poor biocompatibility underscore the urgent need for safer, non-toxic, and eco-friendly alternatives.

Transparent glass ceramics (TGCs) doped with zirconia (ZrO_2) present a promising alternative material[1], [2]. They offer advantages by merging the optical transparency of glass with the enhanced density and strength achieved through controlled nanocrystallization. This combination results in beneficial physical, structural, and biological

*Corresponding author: o.kilicoglu@marmara.edu.tr

characteristics. Consequently, transparent glass ceramics (TGCs) provide a compelling alternative [3]. Their bioactivity, mechanical robustness, transparency, and exceptional biocompatibility make them particularly suitable for biomedical contexts where radiation protection must align seamlessly with patient safety and tissue compatibility.

Zirconium dioxide (ZrO_2) is a valuable addition to glass ceramics due to its high atomic number (Z = 40) and flexible structure[4]. This allows for a denser silicate network without compromising clarity or chemical stability. Additionally, Zr^{4+} acts as a nucleating agent, promoting the formation of tiny tetragonal nanocrystals that improve the glass's resistance to cracking. While some have highlighted these various advantages, they pointed out that information regarding the radiation shielding capabilities of zirconium-containing materials is still limited and varies based on the specific material composition[5].

Innovative bioactive zirconia glass ceramics show considerable promise for use in medical implants, especially in dentistry and orthopedics. Their unique combination of biocompatibility, mechanical strength, and bioactivity makes them suitable for a range of implant applications. Modifying zirconia with hydroxyapatite can enhance its bioactivity, leading to improved integration with natural bone and gum tissues [6], [7]. Composite materials with optimized hydroxyapatite levels can achieve a balance of strong mechanical properties and enhanced bioactivity, making them particularly well-suited for dental implants [7].

In bone repair and regeneration contexts, zirconia composites, especially those enhanced with hydroxyapatite, significantly facilitate early cell adhesion and promote effective osseointegration[8]. Additionally, additively manufactured zirconia tools provide dual functionality as surgical instruments and scaffold structures, improving recovery through targeted drug delivery and mechanical support [9]. Furthermore, zirconia ceramics offer superior aesthetic outcomes in dental restorations, closely mimicking natural tooth appearance and ensuring durability [10].

Despite these promising characteristics, the inherent brittleness of zirconia ceramics poses challenges, emphasizing the necessity for ongoing research to optimize their mechanical properties for high-stress biomedical applications. The continued exploration and development of bioactive zirconia glass ceramics represent significant advancements towards safer, sustainable, and more effective radiation shielding solutions specifically tailored for medical and healthcare settings. There is an increasing number of studies investigating different materials for shielding purposes [11].

This study investigates zirconia (ZrO_2)-doped transparent glass ceramics (TGCs), originally developed and characterized by Mishra et al. to evaluate their potential as advanced radiation shielding materials in biomedical applications, particularly within dental and orthopedic contexts[12]. Based on the SiO_2–Na_2O–CaO–P_2O_5 composition, Mishra et al. incrementally substituted calcium oxide (CaO) with varying molar percentages of ZrO_2 (0 to 6 mol%) to examine how this substitution affects critical physical, structural, and biological properties relevant to radiation protection.

The TGCs synthesized using the conventional melt-quench method exhibited increases in density and structural compactness proportional to the ZrO_2 content. Structural characterizations conducted through X-ray diffraction (XRD) and Fourier-transform infrared spectroscopy (FTIR) revealed significant network modifications, higher density, and reduced particle sizes, indicating enhanced radiation attenuation potential. Further optical characterization and morphological assessments through Field Emission Scanning Electron Microscopy (FESEM) provided deeper insights into structural improvements and optimized optical properties.

Biological evaluations via in vitro cytotoxicity and cell viability assays demonstrated excellent biocompatibility and safety, reinforcing the suitability of these TGCs as effective, environmentally friendly alternatives to traditional lead-based radiation shielding. Building upon the investigation conducted by Mishra et al. (2024), this research elucidates zirconia-doped transparent glass-ceramics (TGCs) as highly promising candidates for sustainable and biocompatible radiation shielding applications within the realm of medical implantology[12]. The aim of this study is to systematically evaluate the radiation shielding characteristics of zirconia-doped transparent glass-ceramics (TGCs) synthesized from the SiO_2–Na_2O–CaO–P_2O_5 compositional framework.

2. Materials and Methods

2.1. Synthesis of Glass Ceramics

Transparent glass ceramics (TGCs) with the specific formulations of $55SiO_2$–$25Na_2O$–$(15-x)CaO$–$5P_2O_5$–$xZrO_2$ (where x = 0, 2, 4, and 6 mol%) were synthesized utilizing the conventional melt-quench methodology, in accordance with previously delineated protocols (Mishra et al., 2024). High-purity chemical precursors—including silicon dioxide (SiO_2, 99%, Sigma Aldrich), disodium oxide (Na_2O, 80%, Sigma Aldrich), calcium oxide (CaO, 95%, Himedia), phosphorus pentoxide (P_2O_5, 98%, Sigma Aldrich), and zirconium dioxide (ZrO_2, ~99%, Sigma Aldrich)—were meticulously weighed, comprehensively mixed utilizing an agate mortar in conjunction with acetone

to ensure uniformity, melted at a temperature of 1350°C for a duration of 1 hour, quenched onto stainless steel molds, subjected to annealing at 450°C for 4 hours, and subsequently cooled gradually to ambient temperature.

Sample Classification:
TGC-BG1: $55SiO_2 + 25Na_2O + 15CaO + 5P_2O_5 + 0ZrO_2$, density = 2.535 g/cm^3
TGC-BG2: $55SiO_2 + 25Na_2O + 13CaO + 5P_2O_5 + 2ZrO_2$, density = 2.633 g/cm^3
TGC-BG3: $55SiO_2 + 25Na_2O + 11CaO + 5P_2O_5 + 4ZrO_2$, density = 2.769 g/cm^3
TGC-BG4: $55SiO_2 + 25Na_2O + 9CaO + 5P_2O_5 + 6ZrO_2$, density = 2.910 g/cm^3

The detailed characterization of these materials, including density, molar volume, optical, structural, and biological properties, were adopted implicitly from Mishra et al. (2024) [12].

2.2. Theoretical expectations and Monte Carlo simulations

The parameters governing the photon interaction were simulated via the PHITS 3.22 Monte Carlo code, which offered detailed elucidation of the time-dependent, continuous-energy transport of particles and photons within a three-dimensional geometry. The geometry employed in the PHITS 3.22 simulations is depicted in Figure 1.

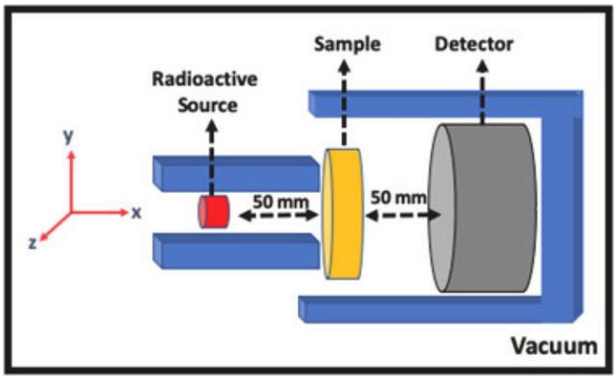

Figure 1. Schematic representation Monte Carlo geometry

In the framework of the simulation configuration, lead blocks were implemented to provide shielding for both the gamma-ray source and the detection apparatus. The detection system was assigned the responsibility of quantifying the photon flux, which was articulated in the units of MeV·cm^2·s^{-1}. These empirical observations were subsequently integrated into the Beer–Lambert law to determine the linear attenuation coefficient, taking into account the specific photon energy and the thickness of the material. For the simulation processes, T-Track tally was employed in the PHITS platform[13]. The particle histories were calibrated to a value of 10^7. The attenuation parameters that were computed were then juxtaposed with those derived from the Phy-X/PSD software. The compositions and densities of the samples were introduced into the Phy-X/PSD system, gamma energy ranges were selected, and computational methods were set accordingly to analyze the shielding performance of TGCs comprehensively across the energy range of 0.015–15 MeV. The Phy-X/PSD software (Şakar et al., 2020), accessible as open-source and online, was specifically designed for radiation shielding and dosimetry calculations. This software was developed using NodeJS v8.4.0, secured with Nginx 1.15.8, and built upon a 256-bit PositiveSSL certification. Detailed information and access to the software are available at: https://phy-x.net/PSD.

The software's versatility enables analysis across a broad gamma photon energy spectrum (0.015–15 MeV), making it suitable for diverse biomedical applications. Its capability to handle a wide variety of materials, coupled with its integration with complementary analytical tools like EPICS2017, XCOM, and MCNPX, ensures reliable and accurate results. Furthermore, Phy-X/PSD's user-friendly interface, customizable reporting options, and comprehensive documentation facilitate straightforward interpretation and dissemination of research findings. Consequently, this software played an essential role in confirming the potential of zirconia-doped TGCs as effective, environmentally friendly radiation shielding materials in medical implantology.

In brief, the software has been shown to produce accurate and reliable results, with good agreement between theoretical and experimental data. This high level of accuracy makes it a trusted tool for radiation shielding analysis[14]. The software calculations required accurate input of the chemical compositions and densities as detailed above and in the referenced work[12].

The gamma photon energy spectrum optimized to 0.015–15 MeV; and within this energy range the LAC, MAC, HVL, TVL, MFP, Zeff and Neff are assessed. The MAC of multi-element materials—such as alloys, minerals, or compounds—can be theoretically estimated using the mixture rule method. The mass attenuation coefficients were determined by the theoretical mixture-rule method, represented mathematically by the following equation:

$$(\mu/\rho)_{material} = \sum_i W_i(\mu/\rho)_i \quad (1)$$

Where respectively W_i and $(\mu/\rho)_i$ represent the weight-fraction and the MAC of the i^{th} element. Elemental weight fractions were calculated as follows:

$$W_i = \frac{n_i A_i}{\sum_j n_j A_j} (2)$$

where n_i and A_i denote the element-number and the atomic-weight of the i^{th} element, respectively.

The mass attenuation coefficient is an intrinsic material parameter that is independent of both the material's density and its physical state[15]. The LAC is a parameter that is contingent upon density and is affected by the physical state of the material; it is determined by the product of the mass attenuation coefficient and the density of the material in question. The following radiation shielding parameters were computed by utilizing the LAC (μ):

$$\text{Half-value layer (HVL): } HVL = \frac{ln2}{\mu} \quad (3)$$

$$\text{Tenth-value layer (TVL): } TVL = \frac{ln10}{\mu} \quad (4)$$

$$\text{Mean free path (MFP): } MFP = \frac{1}{\mu} \quad (5)$$

Further, molecular ($\sigma_{t,m}$), atomic ($\sigma_{t,a}$), and electronic cross-sections ($\sigma_{t,e}$) were determined using mass attenuation coefficients, following these relations:

$$\sigma_{t,m} = \frac{1}{N}(\mu/\rho)_{mater} \sum_i (n_i A_i) \quad (6) \text{ and}$$

$$\sigma_{t,a} = \frac{\sigma_{t,m}}{\sum_i n_i} \quad (7) \text{ and}$$

$$\sigma_{t,e} = \frac{1}{N}\sum_i \frac{f_i A_i}{Z_i}(\mu/\rho)_i \quad (8)$$

The effective atomic number (Z_{eff}) was calculated as[16]:

$$Z_{eff} = \frac{\sigma_{t,a}}{\sigma_{t,e}} \quad (9)$$

Finally, the effective-electron-density can be calculated through the equation below:

$$N_{eff} = \frac{Z_{eff}}{A_{tot}}(N n_{tot}) \quad (10)$$

where A_{tot} and n_{tot} represent the total-atomic-weight and total-number of elements in the material, respectively.

3. Result and Discussion

This study evaluates the gamma radiation attenuation characteristics of various bioactive zirconia (ZrO_2)-doped transparent glass ceramics (TGCs) formulations, each distinguished by their chemical composition and density as outlined in Table 1. The photon interaction properties were examined over an extensive energy range—from 0.015 MeV to 15 MeV—utilizing the The Phy-X/PSD software and PHITS 3.22 Monte Carlo simulation code.

Table 1. Sample code, chemical composition of the investigated TGC (mol %) in SiO_2–Na_2O–CaO–P_2O_5–ZrO_2 system

Sample Name	SiO_2	Na_2O	CaO	P_2O_5	ZrO_2	Density (g/cm^3)
BG1	55	25	15	5	0	2.535
BG2	55	25	13	5	2	2.633
BG3	55	25	11	5	4	2.769
BG4	55	25	9	5	6	2.910

The initial phase of the analysis focused on determining the mass attenuation coefficients (MACs) for the zirconia (ZrO_2)-doped transparent glass ceramics (TGCs) by using the software and simulation codes.

Figure 2 illustrates the variation in mass attenuation coefficients (MACs) of the ZrO_2-doped transparent glass-ceramics (TGCs) against photon energy, while Table 2 lists the corresponding values computed with the Phy-X/PSD software and the PHITS-3.22 Monte Carlo code. The two datasets agree closely. For the best-performing BG4 sample, the MAC drops from 8.040 $cm^2\ g^{-1}$ at 0.015 MeV to 0.022 $cm^2\ g^{-1}$ at 15 MeV, a 99.7 % reduction. At 0.015 MeV, BG4's half-value layer is 0.0030 cm, 16.7 % thinner than BG1 (0.0036 cm), while its density is 2.910 g cm^{-3}, 14.8 % higher than BG1 (2.535 g cm^{-3}), underscoring how ZrO_2 enrichment yields a more compact and efficient shield.

Table 2. μ/ρ ($cm^2 g^{-1}$) results for the glass ceramics.

Energy (MeV)	BG1			BG2			BG3			BG4		
	Phy-X/PSD	PHITS	Dev. %	Phy-X/PSD	PHITS	Dev. %	Phy-X/PSD	PHITS	Dev. %	Phy-X/PSD	PHITS	Dev. %
0.015	7.533	7.526	0.09	7.709	7.716	0.09	7.878	7.882	0.04	8.040	8.044	0.05
0.02	3.309	3.302	0.19	5.104	5.106	0.03	6.828	6.835	0.10	8.483	8.490	0.08
0.03	1.106	1.108	0.15	1.728	1.726	0.15	2.326	2.324	0.10	2.900	2.898	0.05
0.04	0.564	0.569	0.91	0.849	0.849	0.03	1.123	1.123	0.02	1.385	1.384	0.07
0.05	0.369	0.372	0.81	0.522	0.524	0.38	0.669	0.670	0.17	0.810	0.810	0.01
0.06	0.280	0.283	1.01	0.372	0.372	0.22	0.459	0.461	0.33	0.544	0.545	0.21
0.08	0.205	0.206	0.39	0.245	0.245	0.05	0.284	0.284	0.02	0.321	0.321	0.28
0.1	0.174	0.175	0.48	0.195	0.195	0.10	0.215	0.215	0.07	0.234	0.234	0.12
0.15	0.141	0.142	0.39	0.147	0.148	0.54	0.153	0.154	0.42	0.159	0.160	0.28
0.2	0.125	0.126	0.31	0.128	0.128	0.26	0.130	0.131	0.45	0.133	0.133	0.55
0.3	0.107	0.107	0.52	0.108	0.108	0.49	0.108	0.109	0.58	0.109	0.109	0.23
0.4	0.095	0.095	0.31	0.095	0.096	0.65	0.096	0.096	0.43	0.096	0.096	0.32
0.5	0.087	0.087	0.14	0.087	0.087	0.41	0.087	0.087	0.23	0.087	0.087	0.49
0.6	0.080	0.081	0.58	0.080	0.080	0.54	0.080	0.080	0.49	0.080	0.080	0.60
0.8	0.070	0.070	0.20	0.070	0.070	0.35	0.070	0.070	0.29	0.070	0.070	0.44
1	0.063	0.063	0.17	0.063	0.063	0.31	0.063	0.063	0.39	0.063	0.063	0.29
1.5	0.051	0.052	0.93	0.051	0.052	1.34	0.051	0.052	0.87	0.051	0.051	0.29
2	0.044	0.045	0.87	0.044	0.044	0.56	0.044	0.045	1.38	0.044	0.045	1.36
3	0.036	0.037	1.47	0.036	0.036	0.91	0.036	0.037	1.28	0.036	0.036	0.73
4	0.032	0.032	0.19	0.032	0.032	0.85	0.032	0.032	0.93	0.032	0.032	0.82
5	0.029	0.029	1.02	0.029	0.029	0.91	0.029	0.029	0.36	0.029	0.029	0.57
6	0.027	0.027	0.66	0.027	0.027	0.67	0.027	0.027	1.30	0.027	0.027	0.25
8	0.024	0.024	0.28	0.024	0.024	0.15	0.025	0.025	0.78	0.025	0.025	1.39
10	0.023	0.023	0.51	0.023	0.023	0.58	0.023	0.023	0.39	0.024	0.024	1.09
15	0.021	0.021	0.91	0.022	0.022	0.75	0.022	0.022	0.40	0.022	0.022	0.16

Figure 2 presents how the MACs evolve with increasing photon energy. A clear exponential decline is observed, reflecting the inherent relationship between photon energy and attenuation efficiency. The observed behavior is intrinsically dependent on the elemental constituents of the glass ceramics (TGCs) matrices.

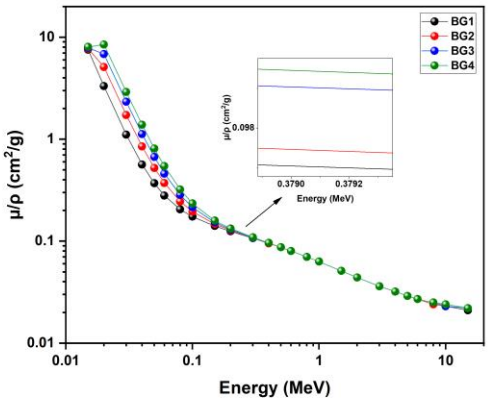

Figure 2. Mass attenuation coefficient of the zirconia doped transparent glass ceramics system with photon energy 0.015 MeV to 15 MeV

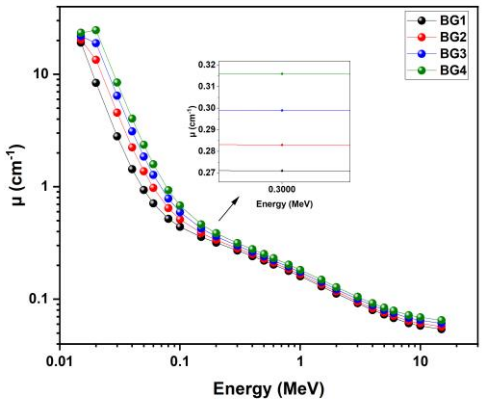

Figure 3. Linear attenuation coefficient of the zirconia doped transparent glass ceramics system with photon energy 0.015 MeV to 15 MeV

At lower photon energies, a pronounced drop in MACs is evident, which becomes more gradual in the intermediate (0.5 – 2 MeV) and higher energy domains (2 – 15 MeV). This phenomenon is associated with the primary mechanisms of photon interactions: photoelectric absorption occurring at lower energy levels, Compton scattering manifesting in the intermediate energy range between 0.5 – 2 MeV, and pair production taking place at elevated energy levels.

The dependencies of these mechanisms are governed by the photon energy (E) and atomic number (Z) of the constituent elements. Specifically, the photoelectric cross-section varies approximately as $E^{-3.5}$ and Z^{4-5}; Compton scattering exhibits E^{-1} and Z dependence; and pair production increases with E and Z^2.

In light of these proportional relationships, the exponential decline in mass attenuation coefficients with increasing photon energy becomes more comprehensible.

As illustrated in Figure 2, the glass-ceramic sample labeled BG4, which contains a high concentration of ZrO_2 in place of a lower CaO content, exhibits higher MACs, particularly in the low-energy region between 0.015 – 0.5 MeV. A more important gamma radiation shielding parameter is the LAC, which combines the MAC with the physical density of the material. Figure 3 illustrates the LACs for each glass ceramic's a function of incident photon energy.

The energy-dependent behavior of LACs show that of the MACs, demonstrating an exponential decline as energy increases. For instance, at 0.015 MeV, the LACs for BG1 through BG4 are calculated to be 19.096, 20.298, 21.815, and 23.398 cm^{-1}, respectively. At 0.6 MeV, these values diminish to 0.203, 0.211, 0.221, and 0.232 cm^{-1}.

It is noted that the disparity between the LACs decreases as the photon energy escalates. This phenomenon can be ascribed to the prevailing mechanisms of photon–matter interactions, as evidenced by the characteristics of the MACs throughout the low, medium, and high energy domains between 2 – 15 MeV. Although all investigated bioactive glasses exhibit effective gamma radiation shielding in the low-energy region between 0.015 – 0.5 MeV, the BG4 sample—characterized by its high LAC and density—demonstrates superior shielding capacity compared to the other compositions. Among the selected glass ceramics, BG4 consistently exhibits the highest LACs, affirming its enhanced gamma shielding capability.

Material thickness plays a critical role in shielding calculations. The thickness required to reduce the intensity of incident photons by 50% is referred to as the HVL, whereas the thickness needed to attenuate the intensity to one-tenth of its original value is known as the TVL. The layer-thickness for reducing the intensity of incident photons to approximately 36.8% of its initial value is termed the MFP. These parameters presents the details of the penetration capabilities of various types of radiation and their interaction with specific materials. Consequently, they are among the most commonly employed metrics for evaluating shielding effectiveness and material performance in radiation protection design. These parameters, plotted in Figures 4 through 6, are inversely related to the LAC.

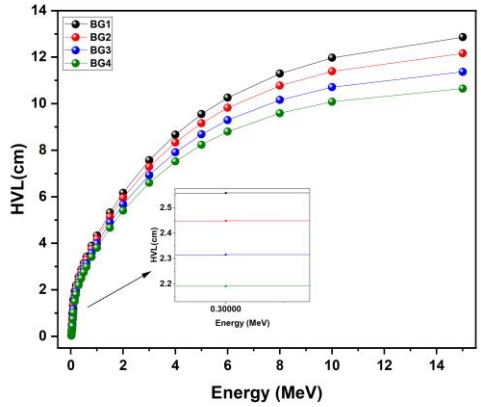

Figure 4. Half value layer (HVL) of the zirconia doped transparent glass ceramics system with photon energy 0.015 MeV to 15 MeV

Across the photon energy spectrum ranging from 0.015 to 15 MeV, HVL-TVL and MFP parameters are elucidated in this inquiry. Figure 4 delineates the HVL measurements of the chosen samples as a function of both photon energy and doping concentration. In a parallel manner, Figures 5 and 6 depict the TVL and MFP values, respectively, for the identical samples under fluctuating photon energies and doping concentrations[17].

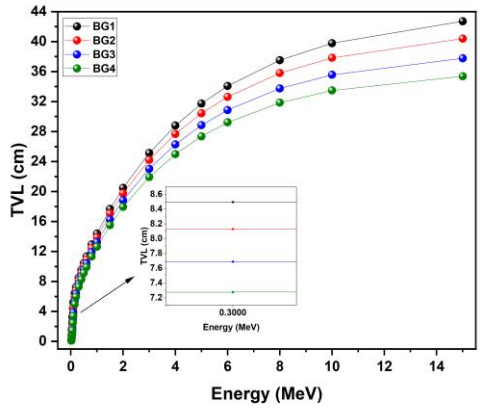

Figure 5. Tenth value layer (TVL) of the zirconia doped transparent glass ceramics system with photon energy 0.015 MeV to 15 MeV

In the range of energies between 0.015-15 MeV, HVL values for BG1 are 0.0036–12.858 cm, 0.0034–12.161 cm for BG2, 0.0032–11.371 cm for BG3, 0.0030-10.649 cm for BG4. The above Figure 4 shows these values. Figure 5 shows that TVL values for BG1, BG2, BG3, and BG4 are 0.121–42.713, 0.113–40.397 cm, 0.106–37.773 cm, and 0.098–35.377 cm in the energy range 0.015-15 MeV. In the energy range between 0.015 to 15 MeV, MFP values for BG1 are 0.052–18.550 cm, 0.049–17.544 cm for BG2, 0.046–16.405 cm for BG3 and 0.043-15.364 cm for BG4. These values can be seen in Figure 6. Lower values of MFP, HVL, and TVL correspond to greater radiation attenuation efficiency. Figure 6 specifically illustrates the MFP values of the glass samples across the photon energy range of 0.015 to 15 MeV.

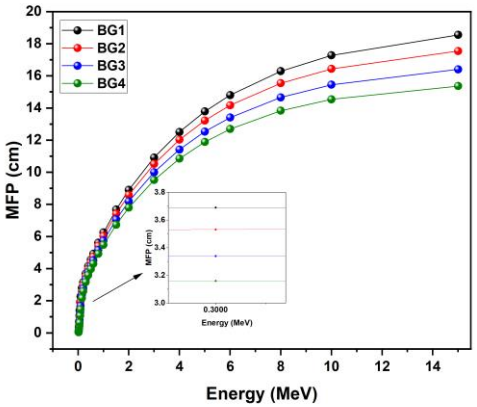

Figure 6. Mean free path (MFP) of the zirconia doped transparent glass ceramics system with photon energy 0.015 MeV to 15 MeV

Among the analyzed specimens, BG4 demonstrates the minimum values for MFP, HVL, and TVL, signifying an exceptional performance in radiation attenuation. The fluctuations in HVL and TVL values across varying photon energies are depicted in Figures 4 and 5. Based on the graphical representations, it is evident that HVL and TVL values exhibit a direct correlation with photon energy, exhibiting an increase concomitant with rising energy levels. Conversely, as photon energy diminishes, the MFP values—conceptually linked to HVL and TVL—also experience a decrease.

Nevertheless, the linear correlation between photon energy and the metrics of MFP, HVL, and TVL alters at energy levels of 10 MeV and beyond. Within this elevated energy spectrum, the values of HVL, TVL, and MFP demonstrate minor variances, as illustrated in Figures 4, 5, and 6.

In the medium to high photon energy domains between 2 – 15 MeV, the impact of chemical composition on shielding efficacy becomes increasingly pronounced. Specifically, the BG1 alloy reveals the highest HVL values, suggesting diminished attenuation efficiency, while the BG4 alloy displays the lowest HVL values, indicative of its superior capability in radiation attenuation. At lower photon energies, variations in energy exert minimal influence on the chemical structure of the shielding materials, contrasting with the more significant effects observed at heightened energies. Consequently, BG4 persistently showcases the lowest HVL, TVL, and MFP values among all specimens. In terms of material density, a higher density is directly correlated with reduced HVL, TVL, and MFP values, thereby indicating an enhanced capability for radiation attenuation.

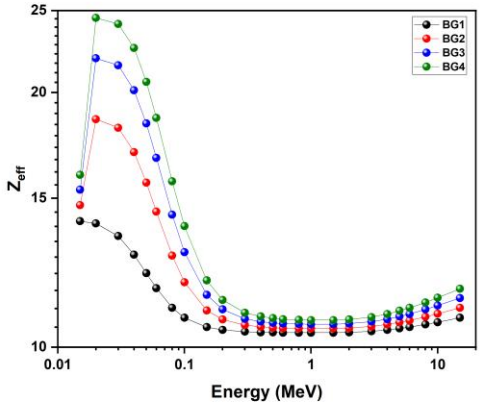

Figure 7. Effective atomic numbers of the zirconia doped transparent glass ceramics system with photon energy 0.015 MeV to 15 MeV

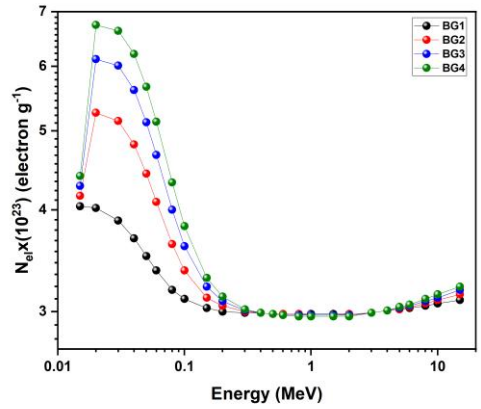

Figure 8. The variation of N_{eff} values with photon energy for the zirconia doped transparent glass ceramics system

Complementing these parameters, Figures 7 and 8 present the theoretical profiles of the Z_{eff} and N_{eff} over the full range of photon energies. Both Z_{eff} and N_{eff} decrease with increasing energy, displaying trends analogous to the MACs[18]. As illustrated in the figure, the Z_{eff}'s of the bioactive glass samples follow the order BG4 > BG3 > BG2 > BG1. Given the direct proportionality between Z_{eff} and N_{eff}, similar trends were observed for both parameters with respect to photon energy and the concentration of the dopant. Among all tested compositions, BG4—reinforced with ZrO_2—demonstrates the most favorable combination of high Z_{eff} and electron density, reinforcing its position as the most effective gamma radiation shielding material within the investigated group.

4. Discussion and Conclusion

This investigation scrutinized the gamma radiation attenuation traits of transparent glass-ceramics blended with zirconia (ZrO_2) across a diverse photon energy spectrum spanning from 0.015 to 15 MeV. Importantly, no previous investigations have systematically evaluated how incremental increases in ZrO_2 concentration—while preserving complete transparency—impact the entire array of photon interaction parameters (MAC, LAC, HVL, TVL, MFP, Zeff, Neff) within this extensive spectrum that spans from diagnostic to therapeutic energy ranges.

The Phy-X/PSD software in conjunction with the PHITS 3.22 Monte Carlo simulation code was utilized for this research. The results indicated that for the glass-ceramics analyzed, the mass attenuation coefficients (MACs), linear attenuation coefficients (LACs), effective atomic number (Zeff), and effective electron density (Neff) exhibited a decrement with the augmentation of photon energy. In contrast, the half-value layer (HVL), tenth-value layer (TVL), and mean free path (MFP) manifested an increment with elevated photon energies. A comprehensive assessment of all computed gamma radiation shielding parameters elucidated that all glass-ceramic specimens exhibited commendable shielding capabilities in the low-energy spectrum, with the BG4 specimen showcasing the most exceptional performance among the evaluated samples.

References

[1] Hussein, K. I., et al. 2022. Optical and radiation shielding properties for novel glass material: $TeO_2/Nb_2O_5/Ta_2O_5/La_2O_3$. *CL*, 19(6), 417-427.

[2] Usman, I., Mohd Sanusi, M. S., Ahmad, N. E., Thabit, H. A. 2024. Optical, thermal, and radiation shielding characterization of bismuth-modified zinc-lithium-tungsten-borate glass. *Physica Scripta*, 99(12), 125972.

[3] Ruengsri, S. 2014. Radiation shielding properties comparison of Pb-based silicate, borate, and phosphate glass matrices. *Science and Technology of Nuclear Installations*, 2014, 1-5.

[4] Beall, G. H., et al. 2017. Zirconia-toughened glass ceramics. Patent WO2017223561A1. https://patents.google.com/patent/WO2017223561A1/en (Erişim Tarihi: 03.05.2025).

[5] Pasiut, K., Partyka, J. 2017. The influence of ZrO_2 addition on the thermal properties of glass–ceramic materials from SiO_2–Al_2O_3–Na_2O–K_2O–CaO system. *Journal of Thermal Analysis and Calorimetry*, 130(1), 343-350.

[6] Xing, Z., Pang, Y., Li, Q. B. E., Zhang, J. Y., Xu, D. 2024. Modification of zirconia with hydroxyapatite for bioactive enhancement as dental implants. *Research Square* Preprint.

[7] Xing, Z., Pang, Y., Li, E., Zhang, J. Y., Xu, D. 2024. Preparation and characterisation of zirconia/hydroxyapatite bioactive composites as potential dental implants. *Journal of Materials Science: Materials in Engineering*, 19(1), 43.

[8] Sivasankar, M. V., Chinta, M. L., Rao, P. S. 2024. Zirconia based composite scaffolds and their

application in bone tissue engineering. *International Journal of Biological Macromolecules*, 130, 558.

[9] Wang, B., et al. 2024. 3D printed zirconia ceramic tool for bone repair with multifunction of drug release, drilling and implantation. *Ceramics International*, 50(18), 33143-33152.

[10] Han, M.-K. 2024. Advances and challenges in zirconia-based materials for dental applications. *Journal of the Korean Ceramic Society*, 61(5), 783-799.

[11] Kılıçoğlu, O., Mehmetcik, H. 2021. Science mapping for radiation shielding research. *Radiation Physics and Chemistry*, 189, 109721.

[12] Mishra, R. K., et al. 2024. Fabrication of bioactive transparent glass ceramics $55SiO_2$–$25Na_2O$–(15-x)CaO–$5P_2O_5$–xZrO_2 ($0 \leq x \leq 6$): physical, structural and in-vitro cell viability insights for biomedical applications. *Ceramics International*, 50(9), 14550-14570.

[13] Özdoğan, H., Kacal, M. R., Kılıçoğlu, O., Polat, H., Öğül, H., Akman, F. 2025. Experimental, simulation, and theoretical investigations of gamma and neutron shielding characteristics for composites reinforced with boron carbide and titanium oxide. *Radiation Physics and Chemistry*, 226, 112167.

[14] Sayyed, M. I., Almuqrin, A. H., Kurtuluş, R., Javier-Hila, A. M. V., Kaky, K., Kavas, T. 2021. X-ray shielding characteristics of P_2O_5–Nb_2O_5 glass doped with Bi_2O_3 by using EPICS2017 and Phy-X/PSD. *Applied Physics A*, 127(4), 243.

[15] Kılıçoğlu, O. 2019. Characterization of copper oxide and cobalt oxide substituted bioactive glasses for gamma and neutron shielding applications. *Ceramics International*, 45(17), 23619-23631.

[16] Kılıçoğlu, O., Tekin, H. O. 2020. Bioactive glasses with TiO_2 additive: behaviour characterization against nuclear radiation and determination of buildup factors. *Ceramics International*, 46(8), 10779-10787.

[17] Kılıçoğlu, O., Tekin, H. O. 2020. Bioactive glasses and direct effect of increased K_2O additive for nuclear shielding performance: a comparative investigation. *Ceramics International*, 46(2), 1323-1333.

[18] Kılıçoğlu, O., et al. 2022. Micro Pb filled polymer composites: theoretical, experimental and simulation results for γ-ray shielding performance. *Radiation Physics and Chemistry*, 194, 110039.